Article no. 26

THE CIVIL ENGINEERING JOURNAL 3-2018

STUDY ON THE SEISMIC PERFORMANCE OF RECYCLED AGGREGATE CONCRETE-FILLED LIGHTWEIGHT STEEL TUBE FRAME WITH DIFFERENT ASSEMBLY JOINTS

Liu Wenchao [1,2], Cao Wanlin [2], Qiao Qiyun [2], Ren Lele [2], Wang Ruwei [2]*

1. *Office of Postdoctoral Research, Beijing University of Technology, Beijing 100124, China; liuwenchao@bjut.edu.cn*
2. *Key Laboratory of Urban Security and Disaster Engineering, Beijing University of Technology, Beijing 100124, China; Email: wanlincao@bjut.edu.cn*

ABSTRACT

In order to investigate the construction of column-to-beam joints and to understand the effect of recycled aggregate concrete (RAC) and cross-section of beams and columns on the seismic performance of recycled aggregate concrete-filled light steel tubular frame structure, four new types of assembly joints were proposed in this paper. A low cyclic loading test of six frame specimens was carried out. The failure characteristic, load bearing capacity, hysteresis property, ductility, strength and stiffness degradation, and energy dissipation were analysed. The damage process of the specimen was simulated using the ABAQUS software, and the results agreed well with those obtained from the experiments. The results showed that the construction pathway of the joints exhibited significant influence on the seismic performance of the frame. The proposed reinforced joint (using angle steel and stiffeners) significantly improved the bearing capacity, stiffness and energy dissipation capacity of the recycled aggregate concrete-filled steel tube frame. The seismic performance of the steel frame was improved, while the energy dissipation capacity increased by 635.7% using RAC filled in the steel tubes. Finally, by appropriately increasing the size of cross-section on the beams and columns can improve the bearing capacity, stiffness and ductility of the structure.

KEYWORDS

Recycled aggregate concrete-filled steel tube frame, Beam-column joints, Assembly structure, Seismic performance, Experimental research, Simulation

INTRODUCTION

Concrete-filled steel tubes (CFST) are widely used in high-rise and super high-rise structures due to the advantages of their high bearing capacity, good ductility, fatigue resistance, and impact resistance [1-4]. Accompanied by the continuous development of material science, as well as the continuous improvement of environmental awareness, recycled aggregate concrete (RAC) has been widely used in light steel frame structures [5-8]. At present, the research on the seismic behaviour of light steel frame structure is mainly focused on the specimens which consist of concrete-filled steel tubular columns and the steel I-beams [9-13]. Previous study [14] showed

that the seismic behaviour of the frame with square concrete-filled steel tube beam was better than that of the frame with steel I - beam. It can be seen that the rectangular concrete-filled steel tube frame structure has more advantages with regards to bearing capacity, seismic performance and material utilization. Therefore, it has the value of further research and application.

In this paper, four kinds of new types of prefabricated beam-column joints were proposed. The square recycled aggregate concrete-filled steel tubes were used as the beam and column of the frame. The beam and column were connected to each other by the bolts. Compared with the traditional steel frame, it has excellent fire resistance and good durability. The influence of joint structure forms, the RAC filling, and cross-section of beams and columns on the load-bearing capacity, stiffness, hysteresis characteristics, and seismic energy consumption of recycled aggregate concrete-filled light steel tubular frame structure were studied. Based on the experimental data, an ABAQUS finite element analysis of the lightweight steel frame was carried out, which provides a data reference for the practical application of the lightweight frames.

TESTS AND METHODS

Design and construction of the specimen.

A single story - single span lightweight steel tube frame and five single story-single-span lightweight steel tube frames filled with recycled aggregate concrete were designed in this paper. The beams and columns of the frame were made of recycled aggregate concrete-filled square steel tube. Herein, the specimens are called FJ-1, FJ-2, FJ-3, FJ-4, FJ-5 and FJ-6, while the design parameters for the specimens are presented in Table 1.

Tab. 1 - Design parameters for the tested specimens

No.	Size of column and beam /mm	Joint structural forms	Concrete strength /MPa
FJ-1	100×100	Angle steel + stiffeners	--
FJ-2	100×100	Angle steel + stiffeners	C40
FJ-3	100×100	Straight steel plate	C40
FJ-4	100×100	U-steel plate	C40
FJ-5	100×100	Angle steel	C40
FJ-6	120×120	Angle steel + stiffeners	C40

The joint structure of specimen FJ-1 is shown in Figure 1, and the production process of the specimens is shown in Figure 2.

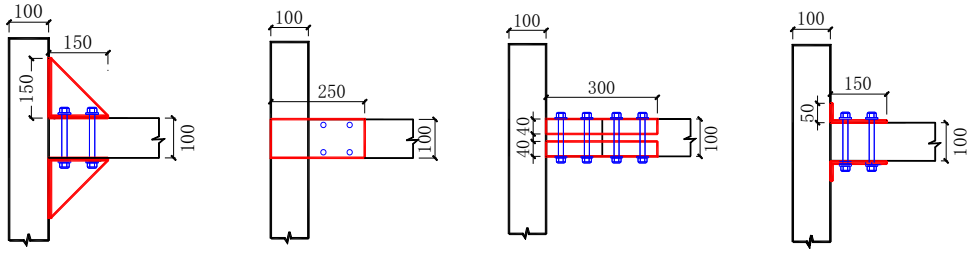

a) FJ-1/FJ-2 Reinforced joint b) FJ-3 Straight joint c) FJ-4 U-steel joint d)FJ-5 Angle joint

(a) Design drawings of different joints

Fig. 1 - Details of the specimen FJ-1 – FJ-6

DOI 10.14311/CEJ.2018.03.0026

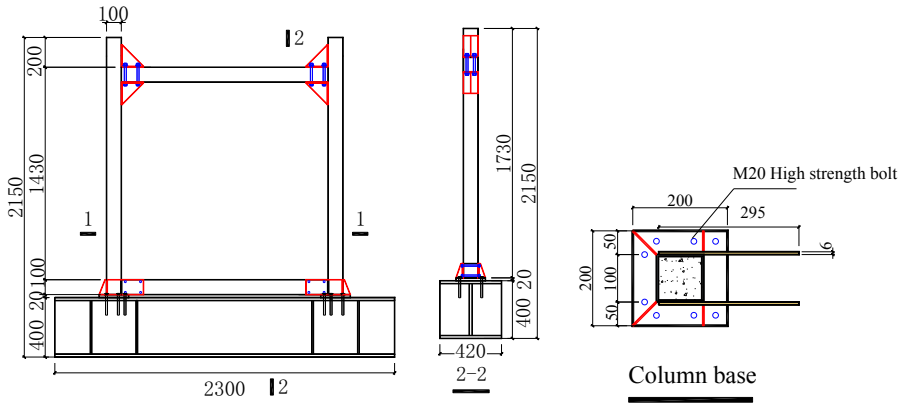

(b) Design drawings of the light steel frame FJ-2

Fig. 1 - Details of the specimen FJ-1 – FJ-6

Before pouring the concrete, the steel tube was fixed on the ground, and the concrete was poured from the top of the steel tube. The concrete was vibrated using a vibrator to ensure the uniformity of the recycled aggregate concrete. Then, the concrete at the top of the column was smoothed. The specimens were maintained under natural conditions for 28 days. Finally, the cover plate was welded at the end of the steel tube to ensure that the steel tube and the concrete worked together during loading. The construction of the specimens is shown in Figure 2.

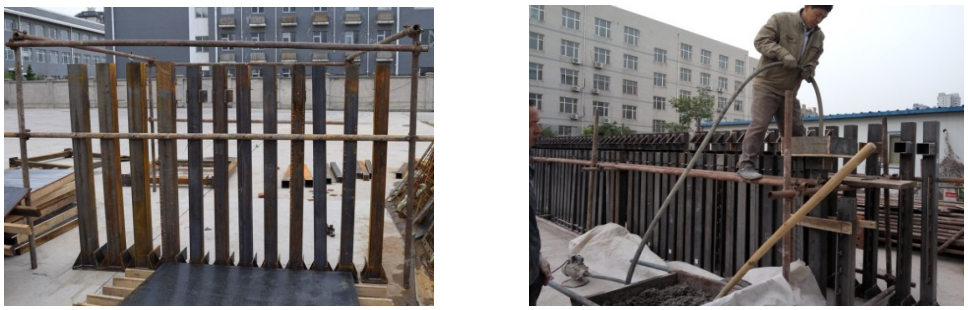

(a) Fabrication of the steel tube *(b) Pouring RAC in the steel tubes*

Fig. 2 - Preparation of the specimens

Material Properties

To ensure the welding quality and the assembly precision, the beams and columns were all made of Q345 steel with wall thickness of 4 mm. In addition, M12 bolts (nominal diameter of 12 mm) were used during the construction. The recycled aggregate concrete was made by mixing the recycled coarse aggregate (particle size of 5 - 10 mm), natural sand, ordinary Portland cement, water, mineral powder, fly ash and water reducer in a certain ratio. Necessary parameters of the recycled coarse aggregate were in accordance with the standard GB/T 25177-2010 [15]. The rate of replacement of the recycled coarse aggregate was 100%. Figure 3 shows the particle size distribution curve of the coarse aggregates in recycled concrete aggregate (RCA). On average, the compressive strength of the standard cubes [16] of the recycled aggregate concrete was 43.8 MPa. The mixing ratios of various components of the recycled aggregate concrete are presented in Table 2.

Tab. 2 - Mixing ratios of various components of the recycled aggregate concrete

Strength Grade	Mix ratio of recycled aggregate concrete kg / m³						
	cement	fly ash	mineral powder	sand	recycled-pebble	water	water reducer
C40	369	79	79	841	841	181	3.5

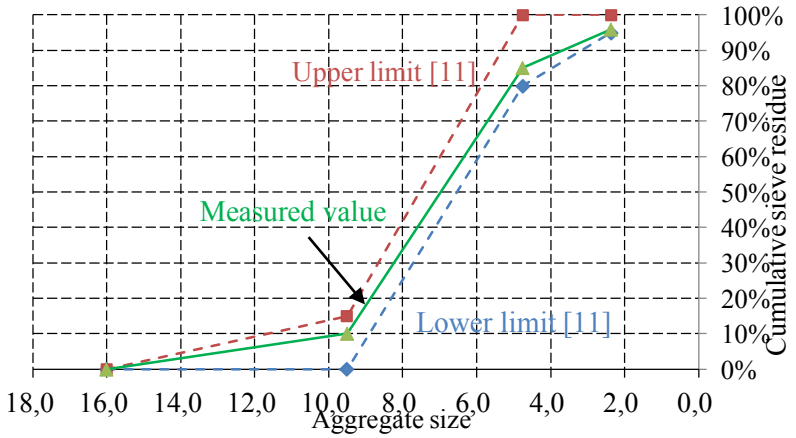

Fig. 3 - Aggregate gradation of the coarse aggregate in RCA

According to the Chinese standard GB/T 228-2002 [17], the mechanical properties of the steel plate used to construct the specimens are presented in Table 3.

Tab. 3 - Measured mechanical properties of the steel

Base metal type	Yield strength /MPa	Ultimate strength /MPa	Modulus of elasticity /MPa
4 mm steel plate	375	477	2.18×10^5

Test Set-Up and Loading

The experiments were carried out at the Integrated Earthquake Engineering Laboratory of the Institute of Engineering Mechanics, China Earthquake Administration, China. Figure 4 shows the scheme and photo of the loading device.

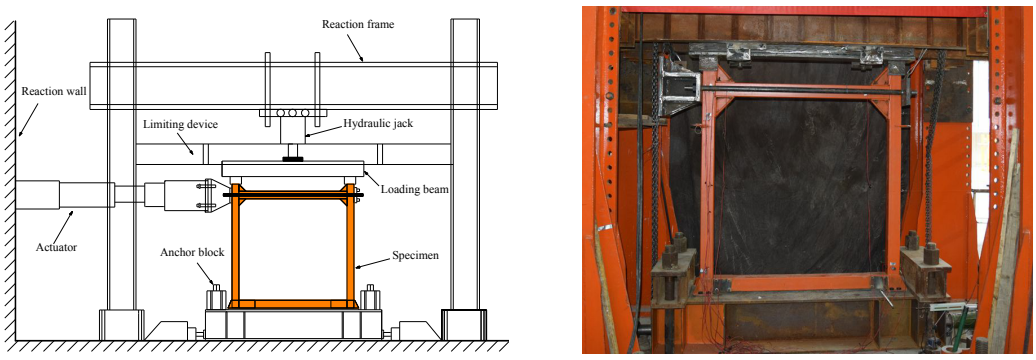

a) Schematic of the loading device *b) Loading field*

Fig. 4 - Schematic and photo of the experimental setup

The repeated low-cycle loading method was used in the experiments. The vertical axial force and the horizontal displacement were controlled by two vertical electro-hydraulic servo loading systems. The axial force was uniformly transmitted to the top of the column through distribution beam. Similarly, the lateral support beams were installed on the two flanks of the distribution beam to prevent the specimen from being out of plane. The column base of the specimen was connected to the I-shaped steel foundation through high strength friction grip bolt. The arrangement of the sensors on the setup is shown in Figure 5.

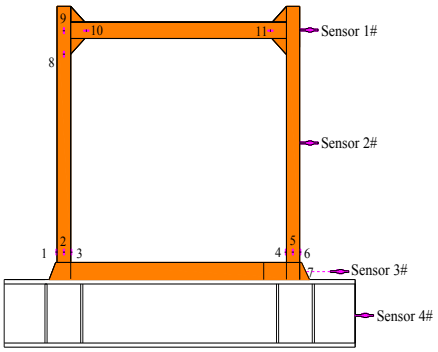

Fig. 5 - Displacement and the strain measuring points on the experimental setup

Loading Program

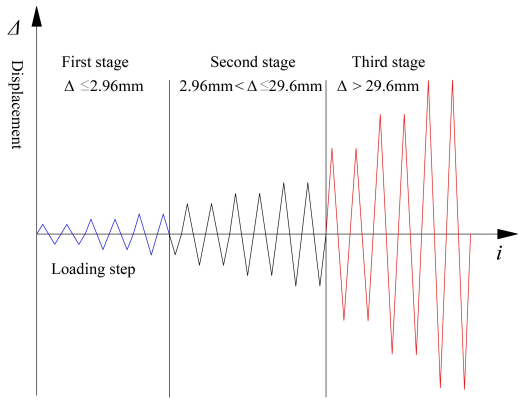

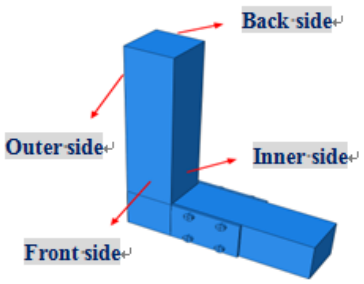

Fig. 6 - Loading protocol

Fig. 7 - Definition of various sections of the column

In the experiment, the vertical load of 600 kN was applied on the loading beam of the specimens. The designed axial compression ratios of FJ-2 - FJ-5 specimens were 0.6, while the vertical axial force was kept constant during the experiments. The horizontal loading process was controlled by the displacement, which could be divided into three stages. (1) The displacement was applied in increments of 1/2500 displacement angle per cycle while the displacement angle was 0 - 1/500. (2) The displacement was applied in increments of 1/500 displacement angle per cycle while the displacement angle was 1/500 - 1/50. (3) The displacement was applied in increments of 1/25 displacement angle per cycle while the displacement angle was equal to 1/50. Each level of the loading displacement had two cycles. When the positive and negative horizontal loads dropped to 85% of the ultimate load of the specimen, the experiment was completed. During the experiment, the loading and unloading rates were same. The loading protocol is shown in Figure 6.

A vertical load of 600 kN was applied to FJ-1 and FJ-6 to ensure the consistency of loading conditions.

RESULTS AND DISCUSSION

Failure Characteristics

This paper defines four sides of the column, namely the front side, inner side, back side and the outer side, as shown in Figure 7. The failure mode of the light steel empty frame FJ-1 is different from the rest of specimens. For the specimen FJ-1, the middle part of the frame beam slightly warped upwards. When the displacement angle reached 1/500, the paint of the column foot slightly wrinkled. When the displacement angle was 1/250, the inner side of the proximal column slightly drummed up. The residual deformation of the proximal column foot occurred, and the steel plate of the column foot yielded when the displacement angle reached 1/83. When the displacement angle was 1/71, the deformation of the inner side of the column foot developed rapidly to about 5 mm. Additionally, the concave deformation of the front side was about 4 mm, while the horizontal load declined rapidly. When the displacement angle was 1/62, the column base of the specimen yielded, and the horizontal load dropped below 85% of the ultimate load. At this point, the experiment was completed, as shown in Figure 8(a).

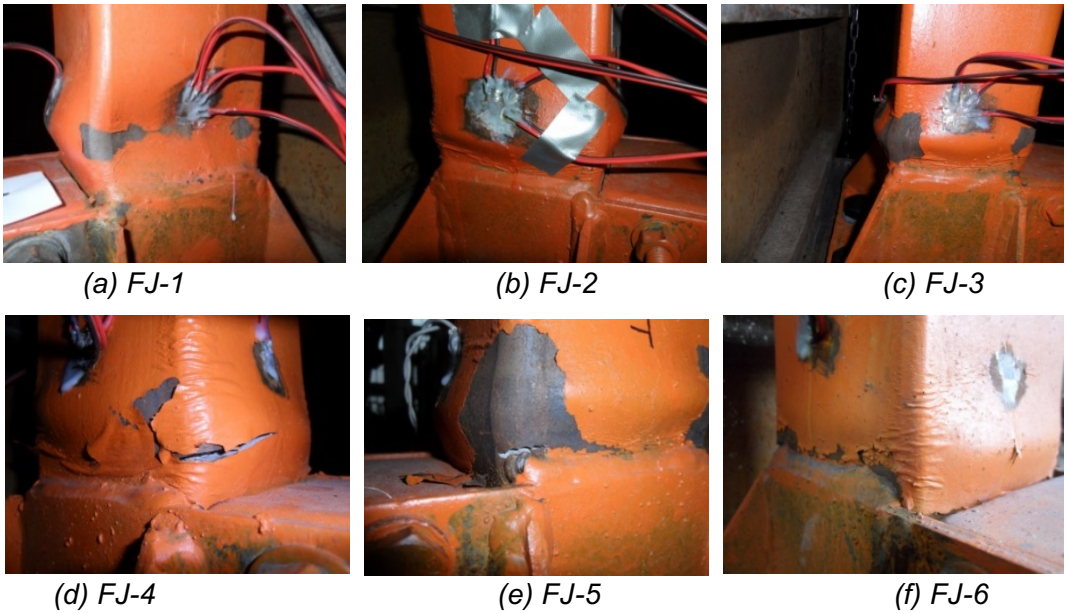

(a) FJ-1 *(b) FJ-2* *(c) FJ-3*

(d) FJ-4 *(e) FJ-5* *(f) FJ-6*

Fig. 8 - Failure modes of the column-base

The failure process of the RAC-filled steel tube frames (Figures 8(b) - 8(f)) was similar. During the loading process, part of the energy was dissipated through the fabricated joints, so that the damage of the frame beam was not significant. For the specimen FJ-3, when the displacement angle reached 1/83, slight hollowing was observed at the beam end. Meanwhile, the recycled aggregate concrete was separated from the steel pipe. When the displacement angle was 1/71, the paint of the bottom part of the column became slightly wrinkled. The bolts in the joint area slightly slid, and the joint plate showed a slight deformation. When the displacement angle was

1/62, the paint in the compression zone of the upper column folded. For the displacement angle of 1/38, the steel plate of the compression zone of the column foot drummed up by about 2 mm, while the fold range of the paint extended to the middle of the cross section of the column. At this moment, the recycled aggregate concrete inside the column was crushed. With the increase in displacement, the drum deformation appeared on both sides of the column foot. When the displacement angle reached 1/18, the steel plate at the bottom of the column tore, and the load dropped rapidly, as shown in Figure 8(c).

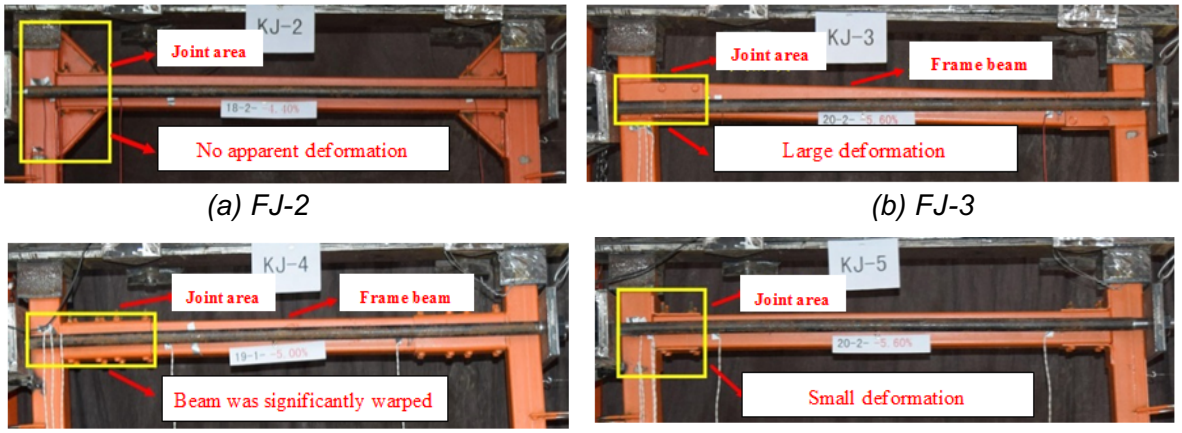

(a) FJ-2 *(b) FJ-3*

(c) FJ-4 *(d) FJ-5*

Fig. 9 - Deformation of beam and column

As seen in Figure 9 the specimens with different assembly joints exhibited different deformations in the joint domain when the specimens were finally destroyed. The specimen FJ-2 adopted the enhanced connection joint structure to expand the joint domain range, while the stiffness of the joint was huge. The joint domain did not show any obvious deformation. Because of the low flexural rigidity of the straight plate joint of FJ-3, the deformation of the joint area was large. The deformation of the frame beam was obvious. The assembly joint of FJ-4 was transferred to the beam end. The joint domain was deformed, and the beam was significantly warped. The joint domain deformation of FJ-5 was smaller in comparison to its large lateral rigidity.

Load-Displacement Response

Herein, F is the horizontal load (F_y is the yield load; F_u is the ultimate load; F_d is the destroyed load, F_d=0.85F_u), for which, the thrust load is positive, while the tensile load is negative. Additionally, Δ is the horizontal displacement (Δ_y is the yield displacement; Δ_u is the ultimate displacement; Δ_d is the destroyed displacement) corresponding to the horizontal load measured using the displacement meter #1. Figure 10 shows the comparison of the force–displacement *(F-Δ)* skeleton curves of the specimens with different parameters.

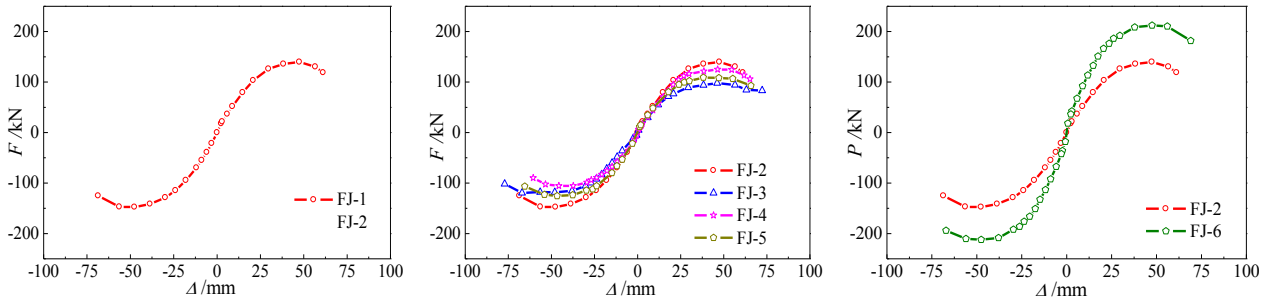

(a) RAC filling *(b) Different joints* *(c) Size of the cross-section*

Fig. 10 - Skeleton curves of the hysteresis plots

As seen from Figure 11(a) that under the same joint form, the ultimate load of the FJ-2 specimen was 100% higher than that of the FJ-1. This is due to the reason that the recycled aggregate concrete slowed down the yield of the steel tube of the specimen, and improved the bearing capacity of FJ-2. As can be seen from Figure 11(b), the bearing capacity of FJ-2 was higher, while the degradation rate of the load was slightly faster than the other specimens in the failure stage. Although FJ-3 had the lowest bearing capacity, its bearing capacity did not decrease significantly after reaching the ultimate load. It shows that the specimen FJ-3 had a good ductility. The ultimate load of the specimen FJ-4 in positive and negative direction exhibited a lager difference, indicating that the specimen was seriously damaged during the loading process. Figure 11(c) shows that the cross-sectional dimensions of the beams and columns had a significant effect on the bearing capacity of the specimens. The downward trend of the bearing capacity of FJ-2 and FJ-6 were basically the same. In this paper, the energy equivalence method was used to determine the yield load and displacement of specimens (see results in Table 4).

Tab. 4 - Measured load and displacement of specimens at characteristic points

No.	F_y/kN	Δ_y/mm	F_u/kN	Δ_u/mm	F_d/kN	Δ_d/mm
FJ-1	65.75	14.98	72.63	17.94	61.74	22.24
FJ-2	120.74	26.83	143.56	47.54	122.03	64.89
FJ-3	91.40	25.75	108.75	56.62	92.44	74.69
FJ-4	98.77	24.40	115.01	46.07	97.75	62.91
FJ-5	97.40	22.55	117.22	42.43	99.64	65.67
FJ-6	184.62	21.07	221.14	47.51	187.96	68.10

Compared with FJ-1, the yield load and ultimate load of FJ-2 increased by 83.6% and 97.7%, respectively. This shows that the core-restrained recycled aggregate concrete can limit the yield of steel tube and increase the bearing capacity of the specimens. The yield loads of FJ-3, FJ-4 and FJ-5 were 24.3%, 18.2% and 19.3% lower than that of FJ-2, respectively. The ultimate loads of FJ-3, FJ-4 and FJ-5 were 24.2%, 19.9% and 18.3% lower than that of the FJ-2. This shows that the different types of assembly joints have a significant influence on the bearing capacity of the concrete-filled steel tube specimens.

Displacement and ductility

In this paper, Δ_d represents the plastic displacement of the specimen, which is the maximum displacement when the horizontal load drops to 85% of the ultimate load. In addition, Δ_y represents the yield displacement, while $\mu = \Delta_d/\Delta_y$ is used to define the displacement ductility coefficient of the specimen. Herein, θ is the displacement angle, $\theta = \Delta$ (horizontal displacement) / h (loading height), the loading height h is 1480mm.The results for these parameters are presented in Table 5.

Tab. 5 - Ductility coefficients of various specimens

No.	Δ_y/mm	θ_y	Δ_u/mm	θ_u	Δ_d/mm	θ_d	μ
FJ-1	14.98	1/99	17.94	1/82	22.24	1/67	1.48
FJ-2	26.83	1/55	47.54	1/31	64.89	1/23	2.42
FJ-3	25.75	1/57	56.62	1/26	74.69	1/20	2.90
FJ-4	24.40	1/61	46.07	1/32	62.91	1/24	2.58
FJ-5	22.55	1/66	42.43	1/35	65.67	1/23	2.91
FJ-6	21.07	1/72	47.51	1/32	68.10	1/22	3.23

1) Compared with FJ-1, the displacement ductility coefficient of FJ-2 increased by 63.5%. It indicates that filling the recycled aggregate concrete in the steel tube can significantly increase the ductility of the structure. This may be due to the reason that the RAC delayed the yielding of the external pipe, and also the development of the plastic hinge of the specimen.

2) Compared with FJ-2, the ductility coefficients of FJ-3, FJ-4 and FJ-5 increased by 19.8%, 6.6% and 20.4%, respectively. This shows that the different types of assembly joints have a great influence on the ductility of the steel tube recycled aggregate concrete frame structure. In short, the ductility of these specimens with different types of joints was better than previously reported.

3) Compared with FJ-2, the ductility coefficient of FJ-6 increased by 33.5%, which shows that increasing the size of cross-section can improve the ductility of the RAC-filled steel tube frame.

3.4. Degradation of the strength

The loading process consists of two loops for each loading displacement The degradation of the strength can be represented by the ratio of peak load of the second cycle (loop) to the peak load of the first cycle (loop) under the same loading displacement. The results for the degradation in strengths for various specimens are shown in Figure 11.

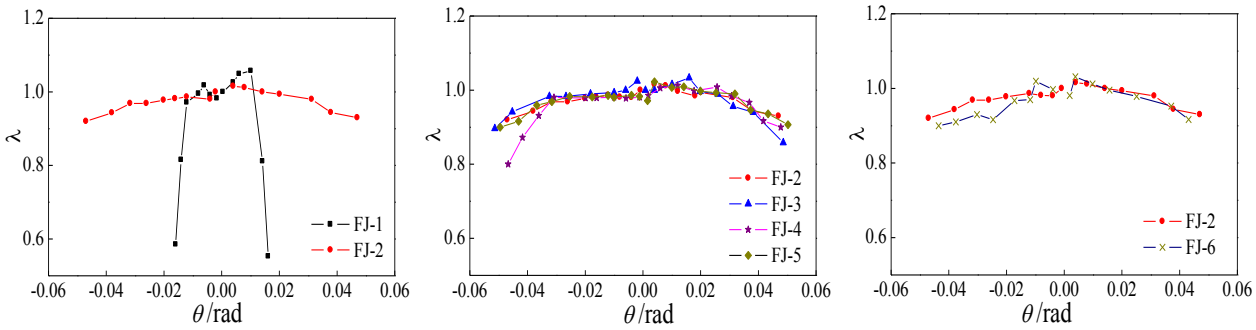

(a) Influence of the RAC filling *(b) Influence of different joints* *(c) Influence of the size of cross-section*

Fig. 11 - Strength degradation curves of various specimens

As can be seen from Figure 11, the strength of the empty steel frame degraded rapidly at the elastoplastic stage, which is mainly due to the buckling of the steel plate of the column base at the failure stage. Meanwhile, the plastic hinge was formed, while the bearing capacity of the frame decreased rapidly. The loading degradation of the RAC-filled light steel tube frames with different assembly joints was similar to each other. The strength under the same loading displacement remained basically unchanged, whereas the trend of the strength degradation after yielding was slow, indicating good ductility. The main reason is that the steel pipe can constrain the deformation of concrete after the concrete is crushed. However, the frame can still maintain high bearing capacity. The size of the cross-section showed little effect on the degradation of strength of various specimens.

Degradation of the stiffness

In this paper, the stiffness degradation feature is represented by the secant stiffness-displacement angle (K-θ) curve, which was obtained from the measured load and displacement at each stage of the specimen. The secant stiffness of each specimen was computed from the skeleton curve of the hysteresis plot using Equation (1).

$$K_i = \frac{\left|F_i^+\right| + \left|F_i^-\right|}{\left|\Delta_i^+\right| + \left|\Delta_i^-\right|} \tag{1}$$

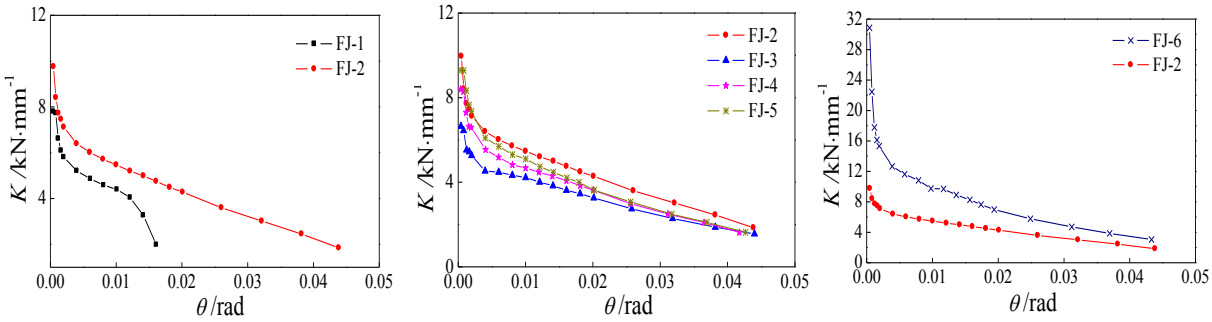

(a) Influence of the RAC filling *(b) Influence of different joints* *(c) Influence of the size of cross-section*

Fig. 12 - Stiffness degradation curves of various specimens.

Figure 12 shows that the stiffness degradations of the RAC-filled steel tube frames were similar to each other. FJ-2 experienced rapid stiffness degradation, while FJ-5 underwent slow stiffness degradation. The rate of degradation of stiffness was relatively fast in the elastic phase, whereas the stiffness degeneration tended to be slow in later stages. The steel tube and the confined concrete can work well in the elastic phase. With the increase in load, the concrete slipped and gradually separated from the steel tube, which degraded the specimen stiffness rapidly. FJ-1 experienced a rapid stiffness degradation process, followed by a slow degeneration process and then, an accelerated degradation process. The stiffness degradation of the steel frame FJ-1 is significantly faster than that of the RAC-filled frame FJ-2, especially in the elastoplastic stage. It shows that filling RAC in the steel tube can obviously slow down the stiffness degradation of specimens at the failure stage. Furthermore, different types of joints have a great influence on the initial stiffness of the RAC-filled steel tube frames. The initial stiffness of the specimen FJ-2 was the largest for the joint's high in-plane flexural rigidity. At the same displacement angle, the initial stiffness of the specimen with straight connection joint was the lowest. At the same displacement angle, increasing the size of beam's cross-section can significantly increase the stiffness of specimens. However, with a larger size of the cross-section of beam and column, the rate of degradation of stiffness of the specimens accelerated.

Energy Dissipation Capacity

The energy dissipation representative value E_P was considered to be the accumulated areas surrounded by the hysteretic curves of the specimens when the load dropped to 85% of the ultimate load. The corresponding results for the energy dissipation are presented in Table 6.

Tab. 6 - Experimental results for the energy dissipation capacities of various specimens

No.	Energy dissipation value E_P/ (kN • m)	Relative value RV
FJ-1	3.206	1.000
FJ-2	23.584	7.357
FJ-3	20.541	6.408
FJ-4	17.101	5.335
FJ-5	20.419	6.370
FJ-6	25.728	8.026

The results show that, compared with the specimen FJ-1, the energy dissipation values of FJ-2, FJ-3, FJ-4 and FJ-5 increased by 635.7%, 540.8%, 433.5% and 537.0%, respectively. Filling RAC can obviously improve the energy dissipation of the steel frame. The energy-dissipation capacity of the specimens with different joints was different, and the energy dissipation of specimen FJ-2 was 15.5% higher than that of FJ-5. The stiffness of the FJ-2 increased the strength of the joint area of the specimen. The energy dissipation capacity of FJ-3 and FJ-5 was similar, while the influence of the two corresponding joint structures on the energy dissipation capacity of the specimen was small. The energy dissipation capacity of FJ-4 was 19.4%, 20.1% and 37.9% lower than those of the FJ-5, FJ-3 and FJ-2, respectively, indicating that the U-steel joint structure contributed less to the energy consumption of RAC-filled steel tube frame. The energy dissipation of FJ-6 was 9.1% higher than that of the FJ-2, which indicates that increasing the cross-sectional dimension of the column and beam can improve the energy dissipation capacity of the specimens.

THEORETICAL CALCULATION AND ANALYSIS

Material constitutive model

Under the confinement of steel tube, the constitutive relation of RAC is quite different from that of the general RAC. Considering the influence of the restraint effect coefficient, the Mander confined concrete model, revised by Yang[18], was used. In this paper, the coarse aggregate replacement rate is considered to be 100%.

In this paper, the elasticity enhancement model (double line model) was used to simulate the reinforcement law. The Mises yield and kinematic hardening criteria were used in the numerical simulation. The stress-strain relationship of the steel bar was simplified as an oblique line. In this study, E's=0.01E_s [19], and the Poisson's ratio was 0.3.

Finite Element Model

ABAQUS software provides a huge library of cells, including solid cells, beam cells, rigid body cells and shell cells [16]. The linear reduction integral 3D solid unit (C3D8R) was used in the modelling of the RAC. The pipe wall thickness was small in the experimental model, so that the shell element (S4R) was used in the modelling of the steel pipe. The model meshing is shown in Figure 13.

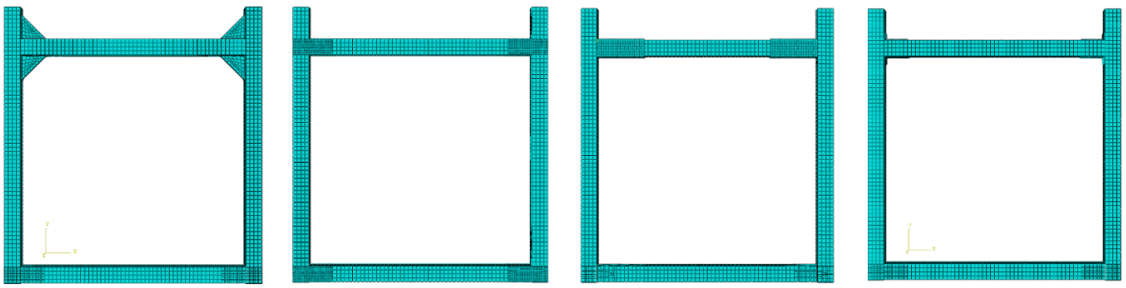

(a) FJ-2 *(b) FJ-3* *(c) FJ-4* *(d) FJ-5*

Fig. 13 - Element mesh of the model

Based on the experimental model, the bottom surface of the column was set as the fixed boundary condition. The vertical load was distributed to the top of the column through the rigid-body load beam with the upper end free. The horizontal displacement was transmitted by the loading beams to make the loading process clear and to improve the convergence of the analysis.

Finite element calculation results and analysis

Comparison of the skeleton curves

Figure 14 shows the comparison between the finite element analysis results and the experimental results of the specimens. It can be seen that the initial stiffness of the finite element simulation is higher than the measured stiffness, which is mainly due to the slight slip of the specimen during the loading test. Compared to the experimental results, the downward trend of the skeleton curves in the finite element analysis is not obvious. This is because the cumulative damage in the numerical analysis was not considered. In general, the calculated results are in good agreement with the experimental results.

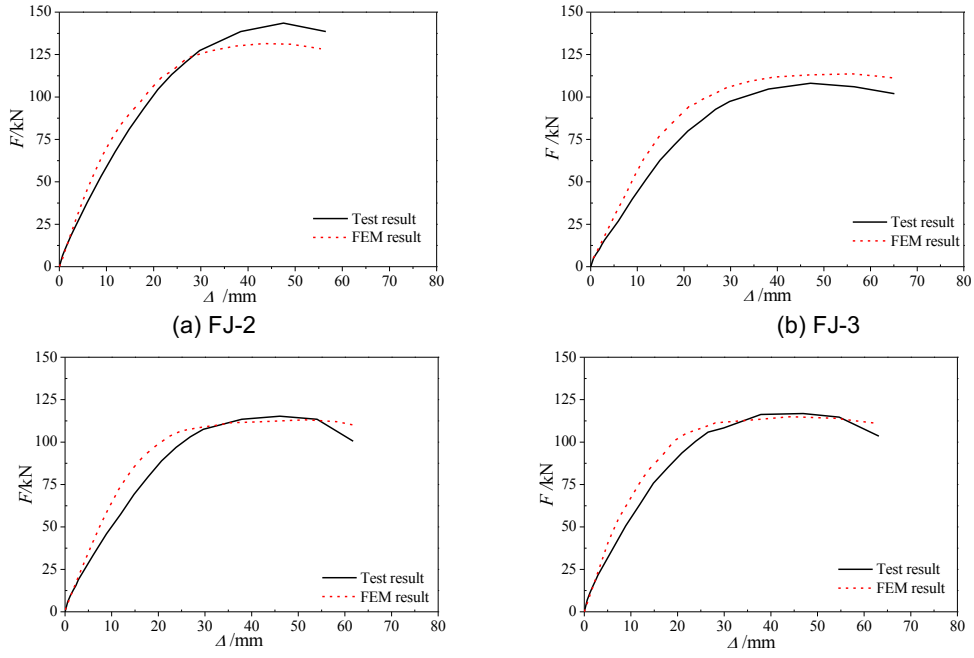

Fig. 14 - Comparison between the measured and calculated results for F-Δ curve

Analysis of stress and damage evolution

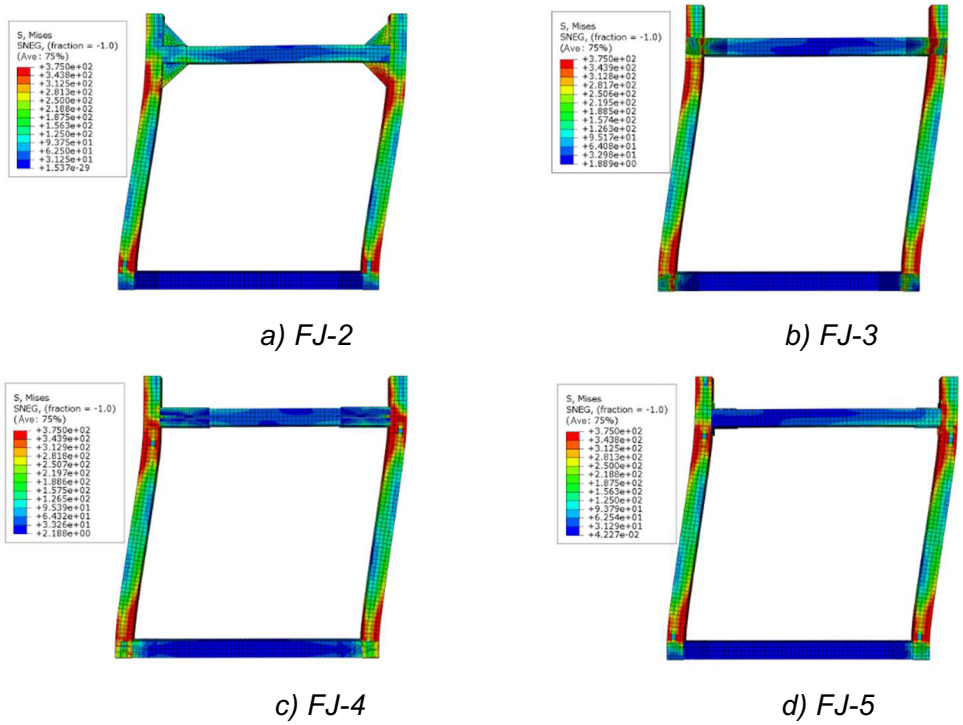

a) FJ-2 *b) FJ-3*

c) FJ-4 *d) FJ-5*

Fig. 15 - Stress cloud of the steel

Figure 15 shows the stress curves of the steel pipe of the four different types of joints when the specimens were damaged. The damage morphology of each specimen was basically similar. Under the action of horizontal loading, the steel pipe was damaged to yield at the top of the column and the column foot. It finally got destroyed. With the different types of joints, the final joint damage came out to be different. It can be seen that the damages of the joints of FJ-2 and FJ-3 were larger, and the damage of joints FJ-4 and FJ-5 were smaller. These results were found to be in accordance with those obtained from the experiments.

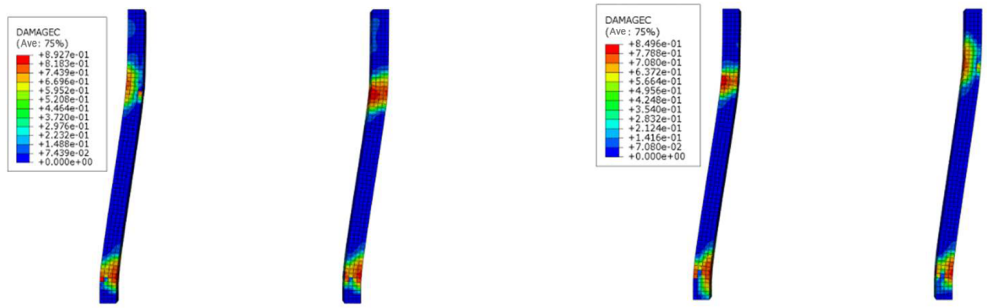

a) FJ-2 *b) FJ-3*

Fig. 16 - Compressional damage of the RCA

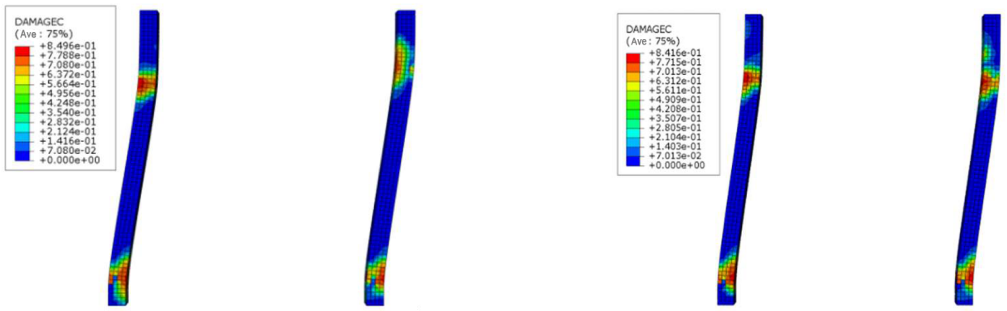

c) FJ-4 *d) FJ-5*

Fig. 16 - Compressional damage of the RCA

Figure 16 shows the plastic damage diagram of the concrete column of the specimens with four different types of joints. It can be seen that, under the action of horizontal load, the concrete in the column foot and join area of the frame was greatly damaged, and finally crushed. The degree of damage of the concrete of the specimen with different joints was different. The damage of FJ-2 under the action of horizontal load was larger. This result was in accordance with the one obtained from experiments.

CONCLUSION

In this paper, the low cycle repeated load tests were carried out on six light recycled aggregate concrete-steel tube frames. The effect of various types of structures of fabricated joints, filled recycled aggregate concrete in the steel tube and sectional dimension of beam and column on the seismic behaviour of the lightweight recycled aggregate concrete (RAC) filled steel tube frame was studied.

(1) Under the same axial compression, filling RAC in the steel tube of the specimen can significantly improve the seismic performance of the steel frame. The ultimate bearing capacity, energy dissipation capacity and displacement ductility coefficient increased significantly.

(2) The failure displacement angles of the specimens with different assembly joints can reach the value of around 1/24, which shows a good structural ductility. The types of joint structures have a significant impact on the failure mode, bearing capacity, energy dissipation capacity and stiffness degradation of the RAC - filled steel tube frame. Among them, the strengthened joint frame has the strongest bearing capacity and the highest energy dissipation capacity. The ductility values of the angle connection joint frame and the straight connection joint frame were good.

(3) Increasing the cross-sectional dimension of the beam and column can significantly improve the bearing capacity, stiffness, ductility and energy dissipation capacity of the lightweight RAC - filled steel tube frame.

(4) Using ABAQUS, a finite element model was developed for the RAC - filled steel tubular frame with different types of the structures of joints. The evolution of the damage to the structure was analysed. The skeleton curve of the finite element model was in good agreement with the experimental results.

ACKNOWLEDGEMENTS

The authors would like to acknowledge the financial support from the Nation Key Research and Development Project (Grant NO. 2017YFC0703304), the China Postdoctoral Science Foundation (Grant NO. 71001015201705) and the Beijing Postdoctoral Science Foundation (Grant NO. Q6001015201702).

REFERENCES

[1] Qiao Q, Wu H, Cao W, et al., 2017. Seismic behavior of bifurcated concrete filled steel tube columns with a multi-cavity structure. Journal of Vibroengineering, 19, 6222-6241.

[2] Ekmekyapar T, Al-Eliwi B J M, Faraj R H, et al., 2017. Performance of lightweight aggregate and self compacted concrete filled steel tube columns. Steel & Composite Structures, 25, 299-314.

[3] Koloo F A, Badakhshan A, Fallahnejad H, et al., 2017. Investigation of Proposed Concrete Filled Steel Tube Connections under Reversed Cyclic Loading. International Journal of Steel Structures, 17, 1-15.

[4] Krishan A L, Chernyshova E P, Sabirov R R., 2018. The Bearing Capacity of the Pre-Compressed Concrete Filled Steel Tube Columns. Defect and Diffusion Forum.

[5] Liu W.C., Cao W.L., Zhang J.W., et al., 2017. Mechanical Behavior of Recycled Aggregate Concrete-Filled Steel Tubular Columns before and after Fire. Materials, 10, 274.

[6] Wang R.W., Cao W.L., Liu W.C., et al., 2017. Experimental study of joint work characteristic of assembly light steel tube frame with recycled concrete-thin wall. Journal of Harbin Institute of Technology, 12, 60-67.

[7] Zheng J., Ozbakkaloglu T., 2017. Sustainable FRP recycled aggregate concrete steel composite columns: Behavior of circular and square columns under axial compression. Thin-Walled Structures, 120, 60-69.

[8] Kadhim I. T., Güneyisi E. M., 2018. Code based assessment of load capacity of steel tubular columns infilled with recycled aggregate concrete under compression. Construction and Building Materials, 168, 715-731.

[9] Zhang A. L., Zhang Z. Y., Jiang Z. Q., et al., 2017. Nonlinear Static Analysis of Repairable Prefabricated Steel Frame Beam-column Joint. Journal of Architecture & Civil Engineering, 4, 1-8.

[10] Fanaie N., Tahriri M., 2017. Stability and stiffness analysis of a steel frame with an oblique beam using method of least work. Journal of Constructional Steel Research, 137, 342-357.

[11] Kawaguchi J., Morino S., Sugimoto T., 1997. Elasto-Plastic Behavior of Concrete-Filled Steel Tubular Frames American Society of Civil Engineers, 272-281.

[12] Rezvani F. H., Behnam B., Ronagh H. R., et al., 2017. Failure progression resistance of a generic steel moment-resisting frame under beam-removal scenarios. International Journal of Structural Integrity, 8, 308-325.

[13] Zhang A. L., Guo Z. P., Liu X. C., et al., 2017. Experimental study on aseismic behavior of prefabricated steel-frame-joits with z-shaped cantilever-beam splicing . Engineering Mechanics, 8, 31-41.

[14] Ricles J. M., Sause R., Peng S. W.; et al., 2002. Experimental Evaluation of Earthquake Resistant Posttensioned Steel Connections. Journal of Structural Engineering, 128, 850-859.

[15] China Standards Publication, GB/T25177-2010, 2011. Recycled Coarse Aggregate for Concrete; Standard Press of China: Beijing, China.

[16] China Standards Publication, GB 50010-2010, 2011. Code for Construction of Concrete Structures; Standard Press of China: Beijing, China.

[17] China Standards Publication, GB/T 228-2002, 2003. Metallic Materials-Tensile Testing at Ambient Temperature;; Standard Press of China: Beijing, China.

[18] Yang Y. F., Wen Z., Dai X. H., 2016. Finite element analysis and simple design calculation method for rectangular CFSTs under local bearing forces. Thin-Walled Structures, 106, 316-329.

[19] Guo, Z.H., Shi, X.D., 2003. Reinforced Concrete Theory and Analyze; Press of Tsinghua University: Beijing, China.

[20] Hibbitt, Karlsson, Sorensen., 2004. ABAQUS/Standard User's Manual, Version 6.4; Hibbitt, Karlsson, Sorensen Inc.: Rawtucket , RI, USA.